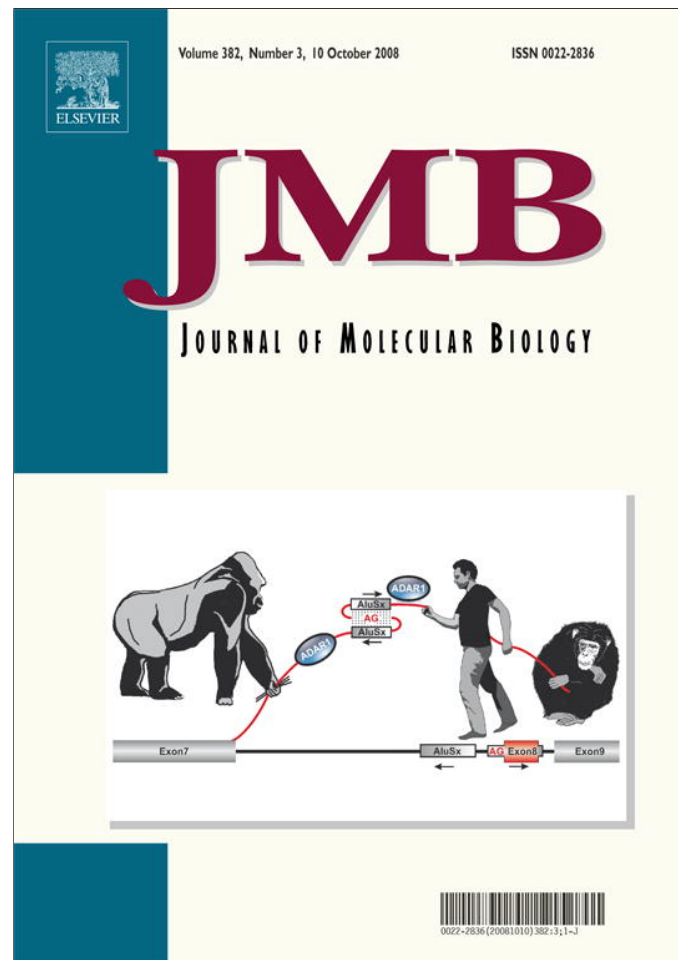


Provided for non-commercial research and education use.  
Not for reproduction, distribution or commercial use.



This article appeared in a journal published by Elsevier. The attached copy is furnished to the author for internal non-commercial research and education use, including for instruction at the authors institution and sharing with colleagues.

Other uses, including reproduction and distribution, or selling or licensing copies, or posting to personal, institutional or third party websites are prohibited.

In most cases authors are permitted to post their version of the article (e.g. in Word or Tex form) to their personal website or institutional repository. Authors requiring further information regarding Elsevier's archiving and manuscript policies are encouraged to visit:

<http://www.elsevier.com/copyright>

**JMB**Available online at [www.sciencedirect.com](http://www.sciencedirect.com)

**ScienceDirect**


# Crystal Structure of the Intact Archaeal Translation Initiation Factor 2 Demonstrates Very High Conformational Flexibility in the $\alpha$ - and $\beta$ -Subunits

Elena Stolboushkina<sup>1</sup>, Stanislav Nikonov<sup>1</sup>, Alexei Nikulin<sup>1</sup>, Udo Bläsi<sup>2</sup>, Dietmar J. Manstein<sup>3</sup>, Roman Fedorov<sup>3</sup>, Maria Garber<sup>1</sup> and Oleg Nikonov<sup>1\*</sup>

<sup>1</sup>*Institute of Protein Research, Russian Academy of Sciences, 142290 Pushchino, Moscow Region, Russian Federation*

<sup>2</sup>*Max F. Perutz Laboratories, Department of Microbiology and Immunobiology, University Departments at the Vienna Biocenter, Dr. Bohrgasse 9/4, A-1030 Vienna, Austria*

<sup>3</sup>*Institute for Biophysical Chemistry, Hannover Medical School, Carl-Neuberg-Strasse 1, D-30625 Hannover, Germany*

Received 22 April 2008;  
received in revised form  
5 July 2008;

accepted 8 July 2008

Available online  
22 July 2008

Edited by K. Morikawa

In Eukarya and Archaea, translation initiation factor 2 (eIF2/aIF2), which contains three subunits ( $\alpha$ ,  $\beta$ , and  $\gamma$ ), is pivotal for binding of charged initiator tRNA to the small ribosomal subunit. The crystal structure of the full-sized heterotrimeric aIF2 from *Sulfolobus solfataricus* in the nucleotide-free form has been determined at 2.8-Å resolution. Superposition of four molecules in the asymmetric unit of the crystal and the comparison of the obtained structures with the known structures of the aIF2 $\alpha\gamma$  and aIF2 $\beta\gamma$  heterodimers revealed high conformational flexibility in the  $\alpha$ - and  $\beta$ -subunits. In fact, the full-sized aIF2 consists of a rigid central part, formed by the  $\gamma$ -subunit, domain 3 of the  $\alpha$ -subunit, and the N-terminal  $\alpha$ -helix of the  $\beta$ -subunit, and two mobile “wings,” formed by domains 1 and 2 of the  $\alpha$ -subunit, the central part, and the zinc-binding domain of the  $\beta$ -subunit. High structural flexibility of the wings is probably required for interaction of aIF2 with the small ribosomal subunit. Comparative analysis of all known structures of the  $\gamma$ -subunit alone and within the heterodimers and heterotrimers in nucleotide-bound and nucleotide-free states shows that the conformations of switch 1 and switch 2 do not correlate with the assembly or nucleotide states of the protein.

© 2008 Elsevier Ltd. All rights reserved.

**Keywords:** ribosome; a/eIF2; translation; initiation; G-protein

## Introduction

In Eukarya and Archaea, translation initiation factor 2 (eIF2/aIF2) is a heterotrimeric GTPase that, in its GTP-bound form, delivers initiator tRNA (tRNA<sub>i</sub>) to the small ribosomal subunit. Pairing between the anti-codon of tRNA<sub>i</sub> and the AUG start codon triggers hydrolysis of GTP, and eIF2/aIF2-GDP is released, leaving tRNA<sub>i</sub> bound in the ribosomal P-site. In contrast to Archaea, in Eukarya, GTP

hydrolysis by eIF2 also requires eIF5, the GTPase activating factor. Eukaryotic eIF2-GDP is recycled to eIF2-GTP with the aid of eIF2B, the guanine exchange factor (GEF), whereas Archaea do not seem to have a special GEF for conversion of aIF2-GDP to aIF2-GTP.<sup>1,2</sup> Thus, the mechanisms for GTPase activation and aIF2-GDP recycling remain poorly understood in Archaea. Like its eukaryotic counterpart eIF2, the archaeal factor aIF2 is formed upon the 1:1:1 association of three subunits:  $\alpha$ ,  $\beta$ , and  $\gamma$ . Subunit, the largest, forms the core of the heterotrimer<sup>3–5</sup> and interacts with both the  $\alpha$ - and  $\beta$ -subunits, whereas the  $\alpha$ - and  $\beta$ -subunits do not interact with each other.<sup>4</sup> In aIF2, the  $\alpha$ - and  $\gamma$ -subunits are required for tRNA<sub>i</sub> binding,<sup>5,6</sup> whereas in eIF2, the  $\beta$ - and  $\gamma$ -subunits are responsible for this task.<sup>3</sup>

The structures of the individual subunits of eIF2/aIF2,<sup>4,7–14</sup> the aIF2 $\alpha\gamma$  dimer of *Sulfolobus solfataricus*,<sup>15</sup> and the aIF2 $\beta\gamma$  dimer of *Pyrococcus furiosus*<sup>16</sup> have been determined. Recently, the structure of an incom-

\*Corresponding author. E-mail address:

[alik@vega.protres.ru](mailto:alik@vega.protres.ru).

Abbreviations used: aIF2, archaeal translation initiation factor 2; EF-1A, elongation factor 1A; eIF2, eukaryotic translation initiation factor 2; GEF, guanine exchange factor; NCS, non-crystallographic symmetry; SsoIF2, initiation factor 2 from *S. solfataricus*; tRNA<sub>i</sub>, initiator tRNA (Met-tRNA<sup>Met</sup>).

plete heterotrimeric aIF2 (the  $\beta$ - and  $\gamma$ -subunits and domain 3 of the  $\alpha$ -subunit) has also been solved.<sup>17</sup> In summary, these studies shaped the view of the structural features of aIF2 and the structure–function relationships in this heterotrimeric protein. Conformational changes in functionally important switch regions of the  $\gamma$ -subunit are of interest and were analyzed in all the known structures. Some differences in conformations of the switches were described and discussed in terms of correlation with the different states of the  $\gamma$ -subunit.<sup>15–17</sup> However, no reliable correlation was observed when a thorough analysis of the known structures of the  $\gamma$ -subunit was performed.<sup>14</sup>

Here, we describe for the first time the crystal structure of the full-sized heterotrimeric initiation

factor 2 from *S. solfataricus* (SsoIF2) at 2.8-Å resolution. Superposition of the four molecules in the asymmetric unit and comparison of the determined structures with the known ones reveal very high conformational flexibility in the  $\alpha$ - and  $\beta$ -subunits, which is probably required for the functioning of aIF2. For the first time, the complete structures of the switch regions of the  $\gamma$ -subunit have been solved at once for four molecules of aIF2 in the asymmetric unit of the crystal, allowing accurate analysis of their conformations. The conformations of the switch regions in the individual  $\gamma$ -subunits were found to differ. Moreover, a comparative analysis of all the known structures of the  $\gamma$ -subunit alone and within the heterodimers and heterotrimer in nucleotide-

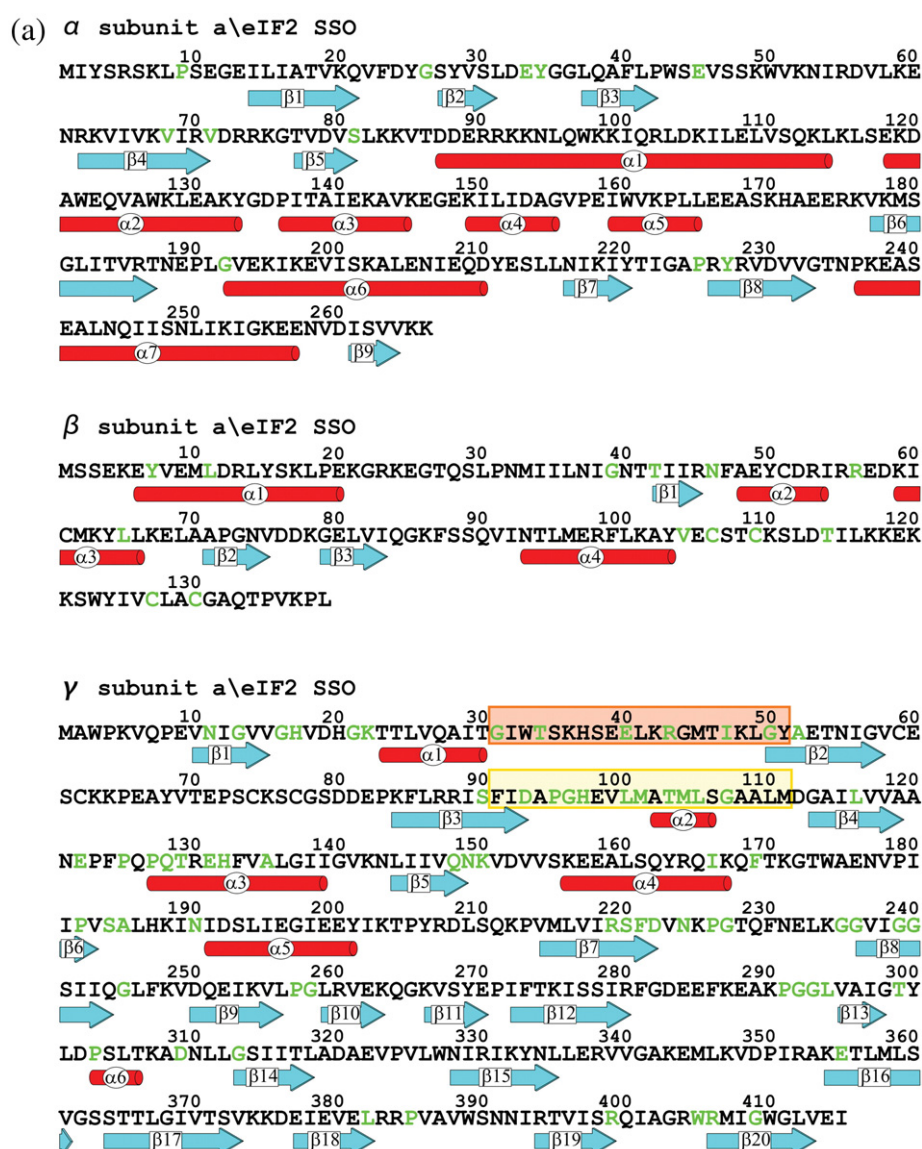


**Fig. 1.** Stereoview of the intact aIF2 $\alpha\beta\gamma$  heterotrimer from *S. solfataricus* and the subunit sequences displaying secondary structure topology. (a) Amino acid sequences of the  $\alpha$ -,  $\beta$ -, and  $\gamma$ -subunits. The numbering and secondary structure elements are indicated. Strictly conserved residues are shown in green. Switch 1 is boxed in orange, and switch 2 is boxed in yellow. (b) Stereo representation of the intact SsoIF2 molecule. The  $\alpha$ -subunit is shown in magenta; the  $\beta$ -subunit, in blue; the  $\gamma$ -subunit, in green; switch 1, in orange; and switch 2, in yellow. (c) Close-up view of the superposition of the switch 1 (orange) and switch 2 (yellow) regions of the heterotrimers in the asymmetric unit of the crystal. Switch 1 of heterotrimer 2 (Table 1) is omitted since its structure is incomplete.

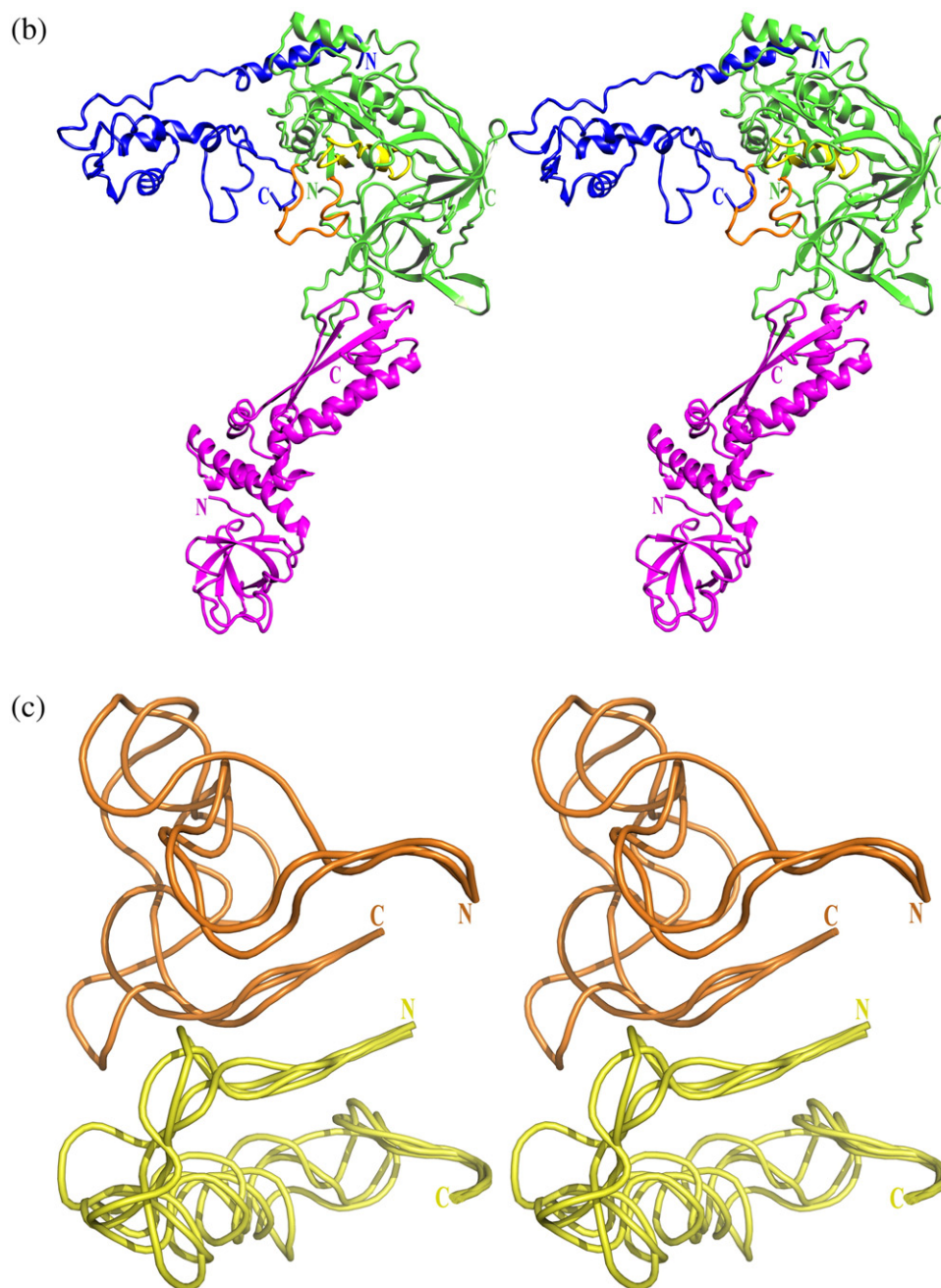


**Fig. 1.** (legend on previous page)

bound and nucleotide-free states shows that the conformations of switch 1 and switch 2 do not correlate with the assembly or nucleotide states of the protein.

## Results

### Overall structure of the aIF2 heterotrimer

A stereoview of the intact aIF2 $\alpha\beta\gamma$  heterotrimer from *S. solfataricus* and its sequence and topology are shown in Fig. 1. The trimeric aIF2 has an L-

shaped conformation, with the  $\alpha$ -subunit comprising most of the long arm, the  $\gamma$ -subunit situated in the angle, and the  $\beta$ -subunit extending the short arm. The G-domain of aIF2 $\gamma$  contacts helix  $\alpha 1$  and the C-terminal region of the  $\beta$ -subunit, whereas aIF2 $\gamma$  domain 2 interacts with domain 3 of the  $\alpha$ -subunit. There is no contact between the  $\alpha$ - and  $\beta$ -subunits. This result is in good agreement with all available biochemical data.<sup>4,5</sup> The most flexible and functionally important regions of aIF2 $\gamma$ , switch 1 and switch 2, are located on the inside of the corner between the  $\alpha$ - and  $\beta$ -subunits. There are four independently refined intact aIF2 heterotrimers in the asymmetric unit of the crystal (Table 1), but only

**Table 1.** Composition of the asymmetric unit of the aIF2 crystal

Heterotrimer	$\alpha$ -Subunit			$\beta$ -Subunit			$\gamma$ -Subunit		
	Chain	Residues	ADP <sup>a</sup>	Chain	Residues	ADP	Chain	Residues	ADP
1	C	1–266	95.5	K	2–129	148.3	A	2–415	105.2
2	D	1–266	102.4	L	2–22	120.6	B	2–35, 46–336, 341–415	104.8
3	G	1–266	93.1	M	2–139	145.7	E	2–415	105.5
4	H	1–265	101.7	N	2–31	135.8	F	2–415	105.2

<sup>a</sup> ADP ( $\text{\AA}^2$ ) is an atomic displacement parameter.<sup>18</sup> Its value is close to that of the usual *B*-factor.

two of them contain the central part and distorted zinc-binding domain of the  $\beta$ -subunits, whereas the N-terminal  $\alpha$ -helices of all these subunits are visible in all heterotrimers. In the crystal, heterotrimers 1 and 2 (Table 1) are situated in alternative layers with heterotrimers 3 and 4. The  $\beta$ -subunits of one layer contact the  $\alpha$ - and  $\gamma$ -subunits of the neighboring layers (Fig. 2). It is interesting to note that the  $\alpha$ - and  $\gamma$ -subunits of the heterotrimers located in the same layers are related by non-crystallographic symmetry (NCS) 2-fold axes, whereas these axes intersect the  $\beta$ -subunit in the N-terminal region of helix  $\alpha 4$ .

### The $\alpha$ -subunit

The overall domain organization of the  $\alpha$ -subunit in the trimeric aIF2 is similar to that described

for the isolated  $\alpha$ -subunit<sup>13</sup> and for that in the aIF2 $\alpha\gamma$  heterodimer.<sup>15</sup> In the crystal, the four  $\alpha$ -subunits in the asymmetric unit have essentially the same structures, with an r.m.s.d. between all C $^{\alpha}$  atoms of less than 1.5  $\text{\AA}$ . Loop  $\beta 3$ – $\beta 4$  (residues 43–62) is the most flexible region of the  $\alpha$ -subunit. The relative positions of domains 1 and 2 are the same in all SsoIF2 molecules, whereas the position of domain 3 deviates slightly ( $\sim 2.0$   $\text{\AA}$ ). Domain 3 retained its position relative to the  $\gamma$ -subunit in all NCS-related structures of SsoIF2. This domain interacts with domain 2 of the  $\gamma$ -subunit through loops  $\beta 6$ – $\alpha 6$  and  $\beta 7$ – $\beta 8$ . Both loops are buried in the cavities on the surface of aIF2 $\gamma$ . The superposition of regions 186–200 and 218–225 contacting the  $\gamma$ -subunit shows their close similarity, with an r.m.s.d. of less than 0.7  $\text{\AA}$  in all four  $\alpha$ -subunits.

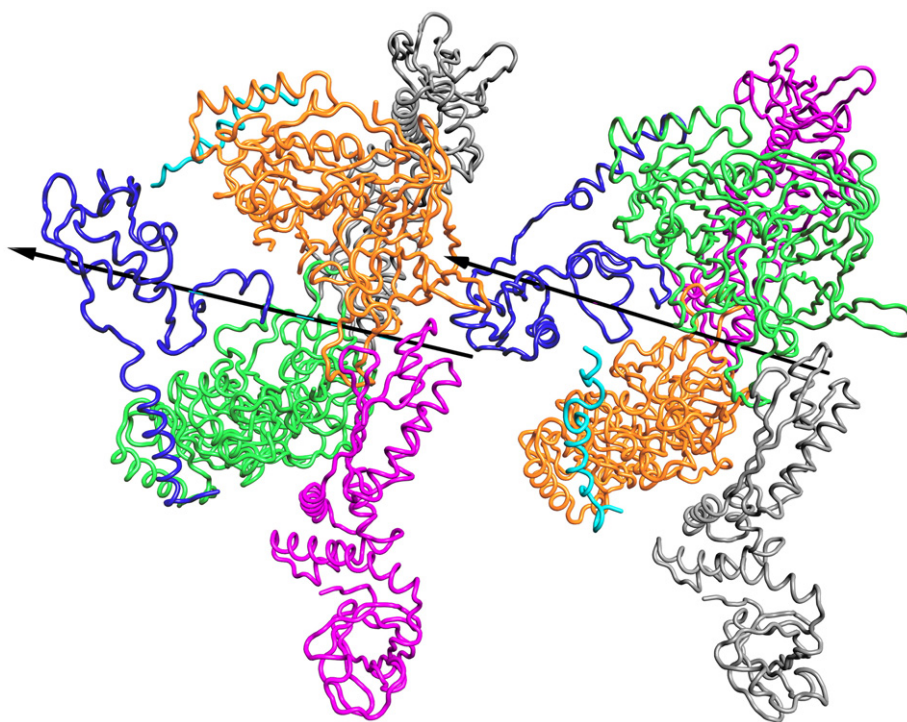


**Fig. 2.** Arrangements of four heterotrimers in the asymmetric unit of the crystal. Heterotrimers 1 and 2 lie in alternative layers with heterotrimers 3 and 4 (Table 1). The  $\beta$ -subunits make inter-layer contacts. The aIF2 $\alpha\gamma$  heterodimers in the same layer are related by local 2-fold axes, whereas helix  $\alpha 4$  of the two  $\beta$ -subunits lies on these axes. In heterotrimers 1 and 3, the  $\alpha$ -subunits are shown in gray; the  $\beta$ -subunits, in dark blue; and the  $\gamma$ -subunits, in green. In heterotrimers 2 and 4, the  $\alpha$ -subunits are shown in magenta; the  $\beta$ -subunits, in pale blue; and the  $\gamma$ -subunits, in gold.

The net of hydrogen bonds between the  $\alpha$ - and  $\gamma$ -subunits is mainly formed by main chain oxygen and nitrogen atoms in two regions separated by more than 12 Å. The first of the regions contains three hydrogen bonds, which result in the formation of a continuous four-stranded anti-parallel  $\beta$ -sheet, including  $\beta 6$ ,  $\beta 7$ , and  $\beta 8$  of the  $\alpha$ -subunit and  $\beta 7$  of the  $\gamma$ -subunit. The second one contains two hydrogen bonds formed by the N-terminus of helix  $\alpha 6$  and loop  $\beta 13$ – $\alpha 6$  of the  $\alpha$ -subunit and loop  $\beta 14$ – $\beta 15$  of the  $\gamma$ -subunit. Possibly, these two regions constitute sites on the aIF2 $\alpha$  and aIF2 $\gamma$  surfaces needed for their recognition and binding.

### The $\beta$ -subunit

Only two of four heterotrimers in the asymmetric unit of the crystal contained the intact  $\beta$ -subunit; in the two other molecules, only the N-terminal  $\alpha$ -helices of the aIF2 $\beta$  were visible. As observed previously in solution<sup>7,10</sup> and in crystal structures,<sup>16,17</sup> this subunit consists of an N-terminal  $\alpha$ -helix connected by a flexible linker to the central  $\alpha$ – $\beta$  domain, which is followed by the C-terminal zinc-binding domain. The whole polypeptide chain was observed only for one  $\beta$ -subunit. The atomic displacement parameters<sup>18</sup> for both subunits are higher than those for the  $\alpha$ - and  $\gamma$ -subunits (Table 1). The  $\beta$ -subunit has a flexible structure with regard to all its parts. The superposition of the N-terminal regions (residues 5–17) produces an r.m.s.d. of 0.73 Å, and the central domains (residues 35–102) can be superimposed with an r.m.s.d. of 3.36 Å, whereas the C-terminal parts of the two  $\beta$ -subunits have different conformations. The zinc-binding pocket in both aIF2 $\beta$  structures is distorted, and no electron

density for the Zn ion is detectable. The mutual arrangements of four cysteine residues, which could be incorporated into this zinc-binding pocket, are also different in both well-detectable  $\beta$ -subunits. In chain M, residue Cys109 makes a disulfide bridge with Cys127 (Fig. 3), whereas in chain K, Cys109 forms a hydrogen bond with Glu25.

The tightest contact between the  $\beta$ - and  $\gamma$ -subunits in the heterotrimer is formed by the N-terminal  $\alpha$ -helix of aIF2 $\beta$  and the region of aIF2 $\gamma$  containing loop  $\beta 5$ – $\alpha 4$ , helix  $\alpha 4$ , loop  $\alpha 4$ – $\beta 6$ , and strand  $\beta 6$ . This contact includes a hydrophobic core and some hydrogen bonds. In addition, there are stacking interactions between side chains of  $\beta$ Tyr7 and  $\gamma$ Tyr163. The great majority of non-polar residues of the inter-subunit core are conserved in all known eIF2/aIF2 $\beta$  structures (Fig. 1a). Several hydrogen bonds stabilize the mutual arrangement of the N-terminal  $\alpha$ -helix of the  $\beta$ -subunit and the corresponding region of aIF2 $\gamma$ , but only one of them, formed by the carbonyl oxygen atom of  $\beta$ Met10 and the ND2 atom of  $\gamma$ Asn190, is strongly conserved and inaccessible to the solvent. The C-terminal part of one  $\beta$  subunit (chain M, residues 134–139) contacts the N-terminal part of switch 1 and loop  $\beta 2$ – $\beta 3$  of the  $\gamma$ -subunit. The inter-subunit hydrophobic core and hydrogen bonds stabilize this contact. The overall surface of interaction between two subunits is 1135 Å<sup>2</sup>, with the C-terminal part of the  $\beta$ -subunit contributing 376 Å<sup>2</sup>. Like in other published structures,<sup>16,17</sup> the contacting surface formed by the C-terminal region of the  $\beta$ -subunit accounts for about 35% of the total interface. In addition, in the crystal, the C-terminal parts of both  $\beta$ -subunits interact with switch 1 of the symmetry-related molecules arranged in the same layers (Fig. 2).

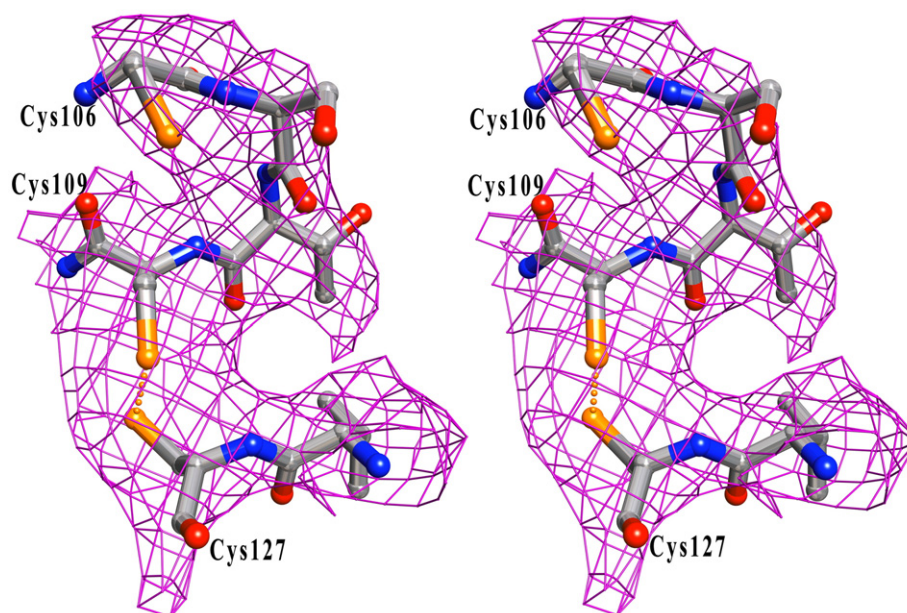


**Fig. 3.** Arrangement of cysteine residues in the distorted zinc-binding domain of the  $\beta$ -subunit (chain M). The electron density is contoured at the  $1\sigma$  level. Cys109 and Cys127 make a disulfide bridge. Cys130 belonging to the  $\beta$ -subunit zinc finger is located apart.

The area of contact between the C-terminal parts of the  $\beta$ -subunit and the  $\gamma$ -subunit in the heterotrimer is small compared with the contact area between aIF2 $\beta$  and symmetry-related heterotrimers. In the crystal, the N-terminal and central parts of the  $\beta$ -subunit interact with all domains of the  $\alpha$ - and  $\gamma$ -subunits of the symmetry-related heterotrimers. Relatively small movements of these domains in the four heterotrimeric structures could result in the configuration flexibility of the central and C-terminal parts of both  $\beta$ -subunits. In the present structure, the crystal contacts fix the  $\beta$ -subunit relative to the  $\gamma$ -subunit in a position that differs from that in other known  $\beta$ - $\gamma$  heterodimers.<sup>16,17</sup> As both well-resolved  $\beta$ -subunits occupy the special positions on the local 2-fold symmetry axes, which relate aIF2 $\alpha\gamma$  heterodimers (Fig. 2), it is impossible to arrange the two other  $\beta$ -subunits in the same manner. Although crystal packing allows the presence of four complete heterotrimers in the asymmetric unit, it is likely that contacts formed by two  $\beta$ -subunits are insufficient to stabilize their positions.

Comparison of the intact aIF2 structures with other structures containing  $\beta\gamma$  heterodimers<sup>16,17</sup> revealed that only the inter-subunit contact formed by the N-terminal  $\alpha$ -helix of the aIF2 $\beta$  is retained. This helix mainly consists of conserved residues and is the most conserved part of the aIF2 $\beta$  structure. Based on these data, we suggest that the  $\beta$ -subunit recognizes the  $\gamma$ -subunit by virtue of its N-terminus. It is interesting to note that in the solution structure of the isolated aIF2 $\beta$ , the N-terminus is disordered.<sup>10</sup> A similar re-organization was observed, for example, for the N-terminus of ribosomal protein L25 in complex with 5S rRNA.<sup>19,20</sup>

### The $\gamma$ -subunit

The  $\gamma$ -subunit forms the core of the heterotrimeric aIF2. The structure of this subunit in the intact heterotrimeric factor is close to that described previously.<sup>4,12,14–17</sup> Four of the NCS-related aIF2 $\gamma$  molecules in the asymmetric unit of the crystal can be superimposed to one another, with an approximately identical r.m.s.d. of 0.9 Å for 348 compared C $^{\alpha}$  atoms. There is no obvious displacement between the G-domain and domains 2 and 3. The most flexible regions of the  $\gamma$ -subunit are switch 1 (residues 31–51), switch 2 (residues 93–113), loop  $\beta$ 1- $\alpha$ 1 (residues 17–21), loop  $\beta$ 15- $\beta$ 16 (residues 338–344), and loop  $\beta$ 19- $\beta$ 20 (residues 399–405). All flexible regions are grouped around the N-terminus of switch 2, and their conformations vary with each molecule.

The polypeptide chains of switch 1 and switch 2 in all the four  $\gamma$ -subunits occupy approximately the same region, but the conformations of these chains differ (Fig. 1c). The most remarkable differences are observed in the N-terminal parts of both switches. Analysis of crystal packing shows that these conformational changes are a result of interactions of switch regions with different mobile parts of their own and symmetry-related heterotrimers.

The regions of domains 2 and G responsible for interactions with the  $\alpha$ - and  $\beta$ -subunits are structurally conserved. In all NCS-related molecules, superposition of the C $^{\alpha}$  atoms constituting the corresponding regions yields a maximum r.m.s.d. of 0.65 Å. Our analysis shows that similar values are typical for superposition of other known aIF2 $\gamma$  structures from different organisms in the nucleotide-free and nucleotide-bound forms.

## Discussion

### Conformations of the switch regions

The structure of the eIF2/aIF2  $\gamma$ -subunit closely resembles the structure of translation elongation factor 1A (EF-1A) in its "active" GTP-bound state.<sup>4</sup> In EF-1A, the conformations of the switch regions correlate with transition from the active GTP-bound state of the protein to the inactive GDP-bound one.<sup>21–23</sup> During the transition, domains 2 and 3 move relative to the G-domain and the conformation of the protein changes from "switch on" to "switch off." Both switch regions attain new conformations, and switch 1 undergoes the most dramatic structural modifications.

In the  $\gamma$ -subunit of aIF2, switch 1 is located on the subunit surface mainly in the groove formed by the G-domain and domain 2, while switch 2 penetrates into the hole comprised by all three domains and bridges the gap between domains G and 3. This hole has a diameter of about 10 Å. Contrary to EF-1A, the "switch off" conformation was not observed in aIF2 $\gamma$  and the groove and hole retain their shapes in all states, thus limiting the conformational changes of both switch regions. The polypeptide chains of switch 1 occupy close positions on the surfaces of aIF2 $\gamma$  in the nucleotide-free, GDP-bound, and GTP-bound forms in all known structures (Fig. 4a), excluding the position in the GDP-bound form of the incomplete heterotrimeric aIF2.<sup>17</sup> In this structure, switch 1 interacts with both switch 2 and the P-loop and its conformation is probably stabilized by a phosphate ion near the nucleotide-binding site. In the absence of such a ligand, switch 1 in aIF2 in the GDP-bound and nucleotide-free forms can adopt close conformations (Fig. 4a). Unfortunately, the complete structures of switch 1 in the GTP-bound form of aIF2 have not yet been determined. Nevertheless, the two incomplete structures of this switch<sup>4,15</sup> in the complexes of aIF2 from *Pyrococcus abyssi* and *S. solfataricus* with Gpp (NH)p demonstrate different conformations. The different contacts between switch 1 and the C-terminal parts of the  $\beta$ -subunit observed in aIF2 $\beta\gamma$  heterodimer and heterotrimers suggest that conformational changes of the  $\beta$ -subunit could affect tRNA binding.

Despite the fact that the  $\gamma$ -phosphate of GTP competes with the N-terminal part of switch 2 and

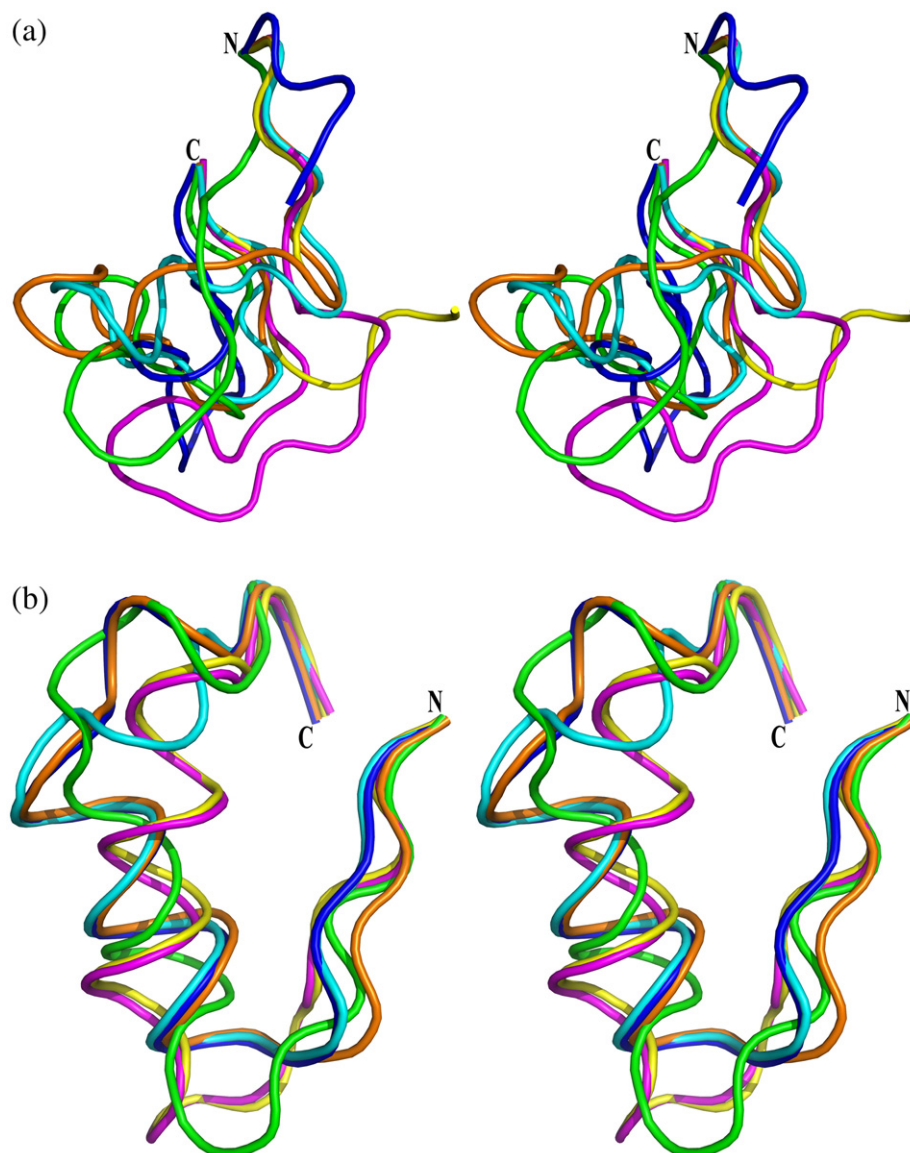


**Fig. 4.** Comparison of switch region conformations of aIF2 $\gamma$  in the nucleotide-free, GDP-bound, and Gpp(NH)p-bound states. Switch regions of nucleotide-free forms are shown in cyan and green; those of GDP-bound forms, in orange and magenta; and those of Gpp(NH)p-bound forms, in blue and yellow. (a) Superposition of switch 1 structures. Data were extracted from PDB files 2PLF, 3CW2, 2QMU, 2PMD, 1KK1, and 2AHO. (b) Superposition of switch 2 structures. Data were extracted from PDB files 1S0U, 3CW2, 1KK3, 2QMU, 1KK1, and 2AHO.

restricts a number of its possible conformations, the superposition of the switch regions of all known structures<sup>4,12,14–17</sup> and the present aIF2 $\gamma$  structure shows no obvious correlation between their conformations and the states of the  $\gamma$ -subunit (Fig. 4b). Indeed, at least the  $\gamma$ -subunit from *Methanococcus jannaschii* and one of the four  $\gamma$ -subunits of the present structure demonstrate that the N-terminal parts of switch 2 can occupy in the nucleotide-free state the same area that they occupy in the GTP-bound state (Fig. 4b). These data also show that switch 2 has the ability to attain spontaneous conformations that permit GTP binding. Nevertheless, as noted previously,<sup>14</sup> such spontaneous GTP binding cannot occur before loop P and switch 2 attain the suitable conformations. In Eukarya, GEF

eIF2B possibly stabilizes suitable conformations of switch 2 and thus gives GTP a preference in the competition with GDP.

#### Conformational flexibility of aIF2

Contrary to EF-1A, there is no visible conformational flexibility in the aIF2 $\gamma$  structure. Moreover, superposition of aIF2 $\alpha\gamma$  and aIF2 $\beta\gamma$  heterodimers<sup>15–17</sup> and the present intact aIF2 structures shows that domain 3 of aIF2 $\alpha$  and the N-terminal helix of aIF2 $\beta$  retain their positions relative to aIF2 $\gamma$  in both nucleotide-free and GDP-bound forms of aIF2. The conformational flexibility of aIF2 that is probably required for its function can be achieved through movement of domains 1 and 2 of aIF2 $\alpha$  (Fig. 5) and

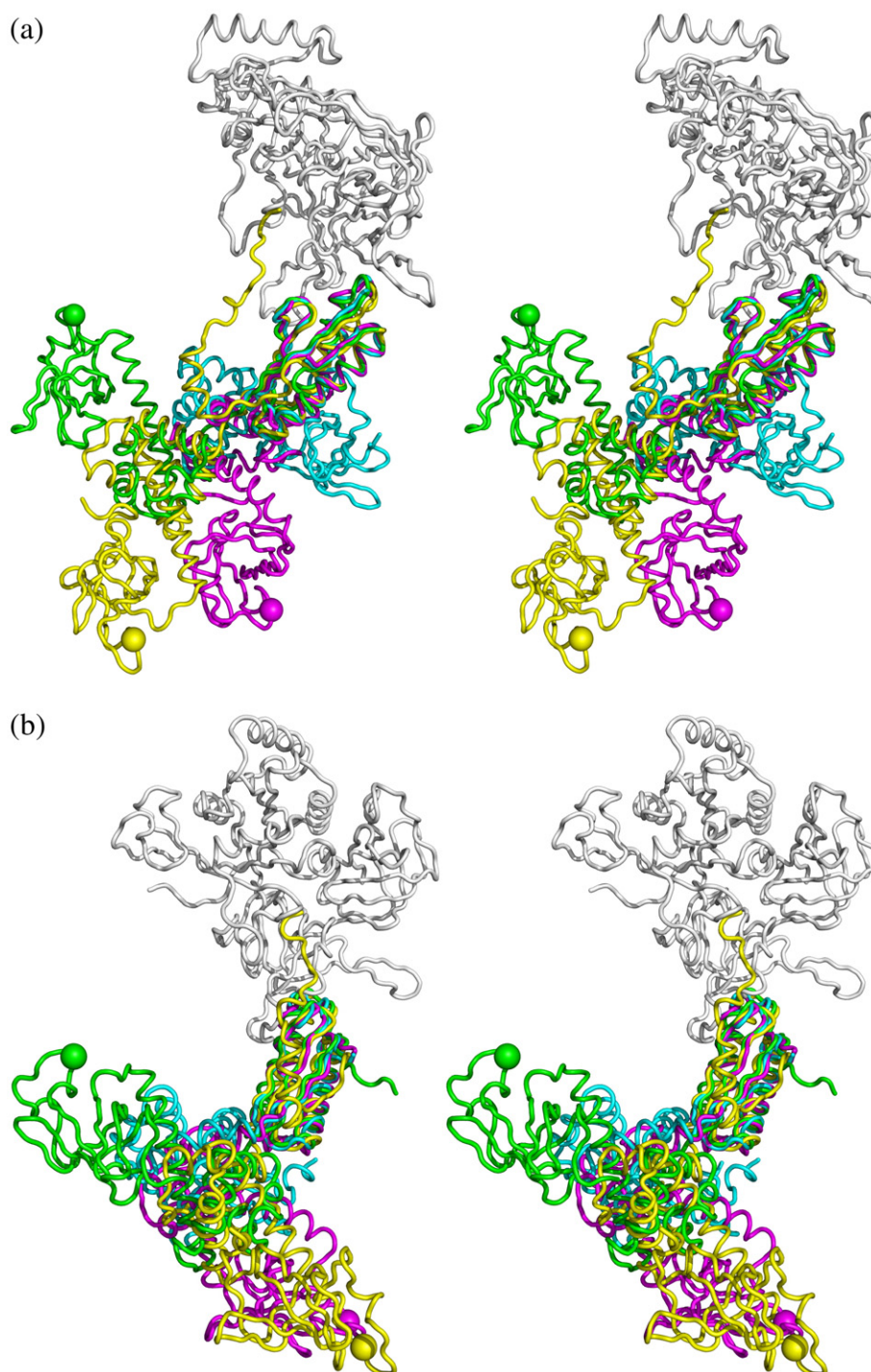


**Fig. 5.** Mutual arrangement of the  $\alpha$ - and  $\gamma$ -subunits. (a) Front view. The  $\alpha$ -subunit from the present structure is shown in magenta; the isolated aIF2 $\alpha$  from *P. abyssi*,<sup>13</sup> in green; the  $\alpha$ -subunit from SsoIF2 $\alpha$  $\gamma$  heterodimer,<sup>15</sup> in light blue; and the human  $\alpha$ -subunit,<sup>11</sup> in yellow. Residue Ser48 of aIF2 $\alpha$  (Ser51 of eIF2 $\alpha$ ) responsible for phosphorylation is indicated by balls. (b) Same as (a) but rotated by 90°. The  $\gamma$ -subunit from the presented heterotrimer is shown in gray.

the central part and the zinc-binding domain of aIF2 $\beta$  (Fig. 6).

In Eukarya, the eIF2 $\alpha$  subunit plays a key role in translational regulation and is a target of specific kinases in response to several stress conditions.<sup>24,25</sup> Amino acid residue Ser51 in eIF2 $\alpha$  has been identified as a phosphorylation site for these kinases. It was

shown that phosphorylation of Ser51 converts eIF2 into a competition inhibitor of eIF2B, which results in strong inhibition of translation initiation.<sup>26,27</sup> This serine residue is conserved in all eukaryal IF2 $\alpha$  sequences but not in archaeal IF2 $\alpha$ . Nevertheless, it was shown that an aIF2-specific kinase from *Pyrococcus horikoshii* can phosphorylate Ser48 within the

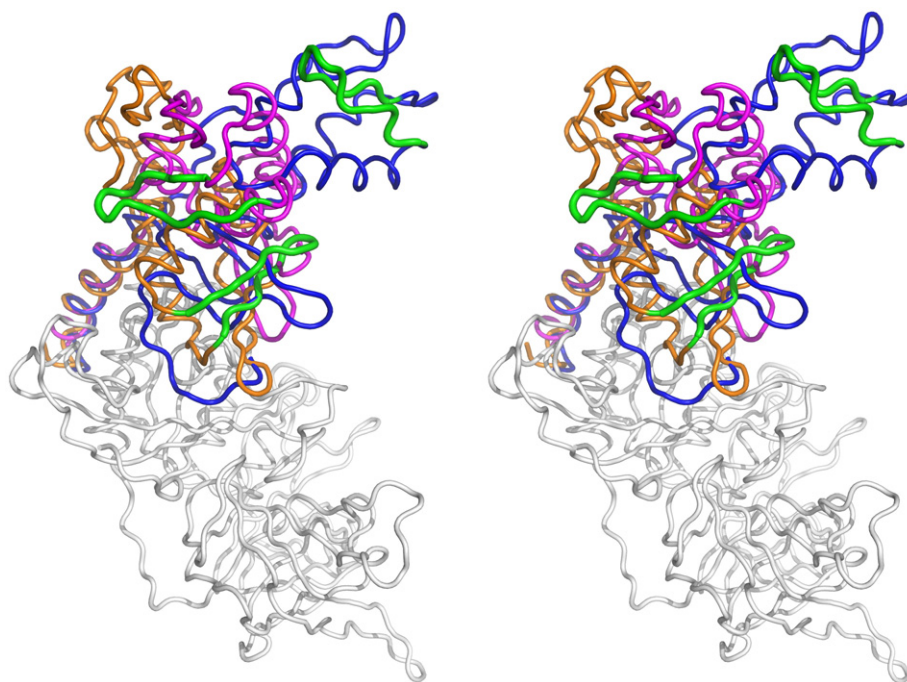


**Fig. 6.** Mutual arrangement of the  $\beta$ - and  $\gamma$ -subunits. The  $\beta$ -subunit from the present structure is shown in dark blue; the  $\beta$ -subunit from *P. furiosus* aIF2 $\beta\gamma$  heterodimer,<sup>16</sup> in orange; and the  $\beta$ -subunit from the incomplete heterotrimer SsoIF2,<sup>17</sup> in magenta. The  $\gamma$ -subunit from the present structure (chain E) is shown in gray. Hairpins  $\beta 2$ – $\beta 3$  are shown in green to show mutual arrangements of central domains from different crystal structures of the  $\beta$ -subunits relative to the  $\gamma$ -subunit.

archaeal IF2 $\alpha$  subunit.<sup>28</sup> Ser51 in the eIF2 $\alpha$  and Ser48 in aIF2 $\alpha$  occupy very close positions in the structure. Domains 1 and 2 of aIF2 $\alpha$  can turn through at an angle up to 180° relative to domain 3. Such rotation takes place in the plane directed at an angle of about 120° to strand  $\beta 6$  of domain 3. In this case, the displacement of Ser48 can achieve 90 Å under favorable conditions. Notably, the strictly conserved Ser44 located in close proximity to Ser48 in aIF2 $\alpha$  is not a site for specific kinases.<sup>28</sup> This could mean that specific kinases contact the flat region on the surface of aIF2 $\alpha$  formed by the long loop  $\beta 3$ – $\beta 4$  (residues 47–65) and the N-terminal part of helix  $\alpha 1$  (residues 83–90). Superposition of these regions of eIF2 $\alpha$ <sup>11</sup> and aIF2 $\alpha$  (present structure) yields an r.m.s.d. of  $\sim 2$  Å. Despite the apparent absence of eIF2B in Archaea, the high mobility of aIF2 $\alpha$  and its potential ability to be phosphorylated could suggest that aIF2 $\alpha$  plays a role in regulation of translation.

Yatime *et al.*<sup>15</sup> suggested an indirect effect of aIF2 $\alpha$  on the affinity of the  $\gamma$ -subunit for tRNA<sub>i</sub>. Superposition of domain 3 of the isolated human eIF2 $\alpha$ <sup>11</sup> and that of the present intact aIF2 structure (Fig. 5) showed that the long C-terminus of eIF2 $\alpha$  (residues 273–302) can contact switch 1 of eIF2 $\gamma$  and may thus affect tRNA<sub>i</sub> binding to eIF2. However, in Archaea, such a function of the C-terminal part of aIF2 $\alpha$  domain 3 is not conceivable: the  $\alpha$ -subunit of aIF2 is shorter (only 266 amino acid residues in SsoIF2) and its domain 3 has no unfolded part and forms one tight contact with the  $\gamma$ -subunit. Moreover, domains 1 and 2 of the  $\alpha$ -subunit of aIF2 do not interact with

the  $\gamma$ -subunit in all observed mutual positions. Based on these data, it is reasonable to conclude that only direct interactions between the  $\alpha$ -subunit and tRNA<sub>i</sub> can account for the role of this subunit in tRNA<sub>i</sub> binding.<sup>5,14</sup> A model for the aIF2 $\alpha\gamma$ -tRNA<sub>i</sub> complex has been proposed in our previous publication.<sup>14</sup> This model demonstrates how the third domain of the  $\alpha$ -subunit can be involved in an extensive direct interaction with tRNA<sub>i</sub>. Moreover, this model shows how the binding specificity for tRNA<sub>i</sub> could be achieved through the interaction of the aIF2 $\alpha$  with a unique ridge formed by two bulged nucleotides on the tRNA<sub>i</sub> surface. Discrimination against all aminoacylated tRNAs except tRNA<sub>i</sub> is a key feature of the IF2. It would be very difficult to explain this feature through an indirect role of the  $\alpha$ -subunit.

The aIF2 $\gamma$  regions responsible for aIF2 $\beta$  binding (residues 152–200 of SsoIF2 $\gamma$ ) were superimposed and the obtained matrices were used to find the corresponding aIF2 $\beta$  positions to determine the mutual arrangements of the  $\beta$ - and  $\gamma$ -subunits in different aIF2 structures. Figure 6 clearly shows that only the N-terminal  $\alpha$ -helical parts of aIF2 $\beta$  (residues 5–17) retain their positions in all known structures. The conformations of the central parts and zinc-binding domains of aIF2 $\beta$  vary in each structure. It is interesting to note that the central part of aIF2 $\beta$  contacts the G-domain of aIF2 $\gamma$  in the *P. furiosus* aIF2 $\beta\gamma$  heterodimer,<sup>16</sup> whereas the zinc-binding domain interacts with close parts of the aIF2 $\gamma$  G-domain in the structures of the truncated<sup>17</sup>

and full-sized (this work) heterotrimeric aIF2 from *S. solfataricus*.

Our analysis revealed that the intact aIF2 structure can be considered as consisting of three parts: a rigid central part and two mobile "wings." The rigid part contains the  $\gamma$ -subunit, domain 3 of the  $\alpha$ -subunit, and the N-terminal  $\alpha$ -helix of the  $\beta$ -subunit. The mobile wings include domains 1 and 2 of the  $\alpha$ -subunit from one side and practically the entire  $\beta$ -subunit from the opposite side. It appears that inter- and intra-subunit interactions in aIF2 cannot ensure its stable conformation. Interactions with external partners are needed to fix the positions of the mobile parts. In crystals, the symmetry-related molecules manifest themselves as such partners. As a result, different crystallization procedures not only produce different crystal forms of aIF2 but also can change the shape of mobile parts of the molecule.

## Materials and Methods

### Overproduction of the $\alpha$ -, $\beta$ -, and $\gamma$ -subunits and purification of the intact SsoIF2 $\alpha\beta\gamma$

The genes encoding the  $\alpha$ -,  $\beta$ -, and  $\gamma$ -subunits of *S. solfataricus* aIF2 were amplified by PCR and cloned in vectors pET11c (for the  $\alpha$ -subunit gene) and pET11d (for the  $\beta$ - and  $\gamma$ -subunit genes). The resulting plasmids were introduced into *Escherichia coli* strain BL21(DE3) (Novagen; for production of the  $\alpha$ - and  $\beta$ -subunits) or C41(DE3) (Imaxio; for production of the  $\gamma$ -subunit). The bacterial strains were grown in LB medium containing 100  $\mu\text{g ml}^{-1}$  of ampicillin. The synthesis of each subunit was induced by addition of IPTG (final concentration = 1 mM), and the cells were harvested 3 h later. The purification of the full-sized Sso-aIF2 $\alpha\beta\gamma$  was performed with some modifications of the procedure described in Ref. 15. The *E. coli* cells were re-suspended in buffer A [10 mM Hepes, pH 7.5, 100 mM NaCl, 0.1 mM ethylenediaminetetraacetic acid (EDTA), and 10 mM 2-mercaptoethanol] and disrupted by sonication. Cellular debris was removed by centrifugation for 20 min at 14,000g. After centrifugation, the supernatants were heated for 20 min at 65 °C. After removal of unstable proteins by centrifugation, the supernatants were mixed and directly loaded onto an S-Sepharose column equilibrated in buffer A. The assembled heterotrimer Sso-aIF2 $\alpha\beta\gamma$  was eluted with a linear gradient of NaCl (100–400 mM) in 10 mM Hepes, pH 7.5, 0.1 mM EDTA, and 10 mM 2-mercaptoethanol. The fractions were analyzed by SDS-gel electrophoresis. The fractions containing all three subunits were pooled and concentrated. The protein solution was diluted with buffer B (10 mM Tris-HCl, pH 8.0, 100 mM KCl, 10 mM MgCl<sub>2</sub>, 1 mM EDTA, and 10 mM  $\beta$ -mercaptoethanol), loaded onto a heparin-Sepharose column equilibrated with buffer B, and then eluted with a linear gradient of KCl (100–500 mM) in 10 mM Tris-HCl, pH 8.0, 10 mM MgCl<sub>2</sub>, 1 mM EDTA, and 10 mM  $\beta$ -mercaptoethanol. Fractions containing pure Sso-aIF2 $\alpha\beta\gamma$  were collected; the protein solution was concentrated to a small volume and finally loaded onto a Superdex 200 column (16 mm  $\times$  60 cm; Amersham) equilibrated with buffer C (10 mM Tris-HCl, pH 8.0, 200 mM KCl, 0.3 mM EDTA, and 2 mM 1,4-dithiothreitol). Fractions containing homogeneous Sso-aIF2 $\alpha\beta\gamma$  protein (as judged by UV spectral analysis and non-denaturing PAGE) were pooled and concentrated.

### Crystallization of the intact SsoIF2 $\alpha\beta\gamma$

All crystallization trials were carried out at 22 °C using the hanging-drop vapor-diffusion technique by mixing 2.0  $\mu\text{l}$  of the protein solution (10–20 mg ml<sup>-1</sup> of Sso-aIF2 $\alpha\beta\gamma$  in buffer C) with 2.0  $\mu\text{l}$  of reservoir solution [100 mM Tris-HCl, pH 8.5, 720 mM sodium formate, 9% PEG (polyethylene glycol) 8000, and 9% PEG 1000] and 1.0  $\mu\text{l}$  of 5% monomethyl ether PEG 5000 as an additive. Crystals appeared after 2–3 days and reached maximum dimensions of 600  $\mu\text{m} \times 200 \mu\text{m} \times 40 \mu\text{m}$  within 1 week. Cryoprotection of the crystals was achieved by adding ethylene glycol to the reservoir solution to a final concentration of 15% (v/v).

### Data collection, structure determination, and refinement

X-ray diffraction data were collected employing synchrotron radiation at the X12 beamline at DESY (Hamburg, Germany) using the MAR CCD detector. The data were processed and merged with the XDS program suite.<sup>29</sup> An analysis of diffraction data suggested that the crystal had an orthorhombic symmetry. A molecular replacement solution was obtained with the program PHASER<sup>30</sup> using space group *P*2<sub>1</sub>2<sub>1</sub>2. The structure of aIF2 $\gamma$  in the apo form was used as a search model [Protein Data Bank (PDB) code 2PLF]. The unique solution was found and used to calculate an initial electron density map. The quality of the map was sufficient to build the  $\gamma$ - and  $\alpha$ -subunits of two aIF2 molecules in the asymmetric unit. The  $\beta$ -subunit was not visible. The model was subjected to several rounds of computational refinement and map calculation with Crystallography & NMR System<sup>31</sup> as well as manual model inspection and modification with O.<sup>32</sup> However, we could not confidently detect the  $\beta$ -subunit exclusive of its N-terminal  $\alpha$ -helix and refine this model to an *R*-free value less than 40%. Detailed analysis of the experimental data showed that the crystals of intact aIF2 are twinned and

**Table 2.** Data collection and refinement statistics

<i>Data collection</i>	
Beamline	X12 DESY
Wavelength (Å)	0.84230
Space group	<i>P</i> 2 <sub>1</sub>
Unit cell	
In angstroms	79.20, 162.92, 161.28
In degrees	90.0, 90.04, 90.0
Unique reflections	95,812
Resolution (Å)	20.0–2.80 (2.85–2.80)
Completeness (%)	95.3 (90.9)
Redundancy	3.19 (3.25)
<i>I</i> / $\sigma$ ( <i>I</i> )	10.71 (2.26)
<i>R</i> <sub>merge</sub> (%)	6.9 (54.5)
<i>Refinement</i>	
Resolution range (Å)	20.0–2.80
Twin law	<i>h</i> , $-k$ , $-l$
Twin fraction	0.459
<i>R</i> <sub>work</sub> / <i>R</i> <sub>free</sub> (%)	22.5/27.6
No. of protein atoms	23,825
r.m.s.d. bond length (Å)/angles (°)	0.002/0.365
Wilson <i>B</i> -factor (Å <sup>2</sup> )	71.9
Average ADP <sup>a</sup> for all atoms (Å <sup>2</sup> )	106.8

Values in parentheses are for the highest-resolution shell. *R*<sub>free</sub> factors were calculated for 5.0% randomly selected test sets that were not used in the refinement.

<sup>a</sup> Atomic displacement parameter.<sup>33</sup>

that they belonged to the monoclinic symmetry system with four aIF2 molecules in the asymmetric unit. The cumulative intensity distribution calculated with DETWIN of the CCP4 program suite<sup>33</sup> indicated pseudo-hemihedral twinning in space group  $P2_1$ . The twin law  $h, -k, -l$  describes a real space rotation about axis  $a$  of the unit cell. The twin fraction was estimated to be 0.367. The previously determined structure of aIF2 $\alpha\gamma$  was used as a search model to find unique positions of all heterodimers in this space group. The unique solution was found also with the program PHASER and twinned data.

At the next stage of structure determination, the program suite PHENIX<sup>18</sup> was used. The twin fraction calculated by this program increased noticeably and was estimated to be 0.465. The electron density calculated after several rounds of refinement and manual model modification allowed us to build the  $\beta$ -subunits in two NCS-related molecules of the aIF2 factor. These  $\beta$ -subunits occupy positions on the local 2-fold axes, which connect the aIF2 $\alpha\gamma$  heterodimers in the asymmetric unit. At the final step of the refinement, the translation–libration–screw procedure was used.

The final model, refined to an  $R$ -free factor of 27.6% and an  $R$ -factor of 22.5% at 2.8-Å resolution, includes 3023 amino acid residues. Data and refinement statistics are summarized in Table 2. NCS restraints were used during the early stages of refinement, but, finally, all four aIF2 molecules in the asymmetric unit were refined separately. The model bias present in the initial molecular replacement solution was tackled using composite omit, cross-validated, and  $\sigma_A$ -weighted maps implemented in Crys-tallography & NMR System.

#### PDB accession number

The coordinates and structure factors for the crystal structures of the intact aIF2 $\alpha\beta\gamma$  have been deposited in the PDB under ID code 3CW2.

#### Acknowledgements

This research was supported by the Russian Academy of Sciences, the Russian Foundation for Basic Research (05-04-48696), the Program of Russian Academy of Sciences on Molecular and Cellular Biology, and the Program of the Russian Federation President in support of outstanding scientific schools. The research of O.N. was supported by International Association for the promotion of cooperation with scientists from the New Independent States of the former Soviet Union through grant no. 05-109-4979, and that of M.G. was supported, in part, by an International Research Scholar's award from the Howard Hughes Medical Institute. The work in U.B.'s laboratory was supported by the Austrian Science Fund through grant no. 15334. D.M. acknowledges the Fonds der Chemischen Industrie. We thank David Hasenöhrl for his support in cloning.

#### References

- Hinnebusch, A. G. (2000). Mechanism and regulation of initiator methionyl-tRNA binding to ribo-

- somes. In *Translational Control of Gene Expression* (Sonenberg, N., Hershey, J. W. B. & Mathews, M. B., eds), pp. 185–244, Cold Spring Harbor Laboratory, Cold Spring Harbor, NY.
- Dever, T. E. (2002). Gene-specific regulation by general translation factors. *Cell*, **108**, 545–556.
- Flynn, A., Oldfield, S. & Proud, C. G. (1993). The role of the beta subunit of initiation factor eIF-2 in initiation complex formation. *Biochim. Biophys. Acta*, **1174**, 117–121.
- Schmitt, E., Blanquet, S. & Mechulam, Y. (2002). The large subunit of initiation factor aIF2 is a close structural homologue of elongation factors. *EMBO J.* **21**, 1821–1832.
- Pedulla, N., Palermo, R., Hasenöhrl, D., Bläsi, U., Cammarano, P. & Londei, P. (2005). The archaeal eIF2 homologue: functional properties of an ancient translation initiation factor. *Nucleic Acids Res.* **33**, 1804–1812.
- Yatime, L., Schmitt, E., Blanquet, S. & Mechulam, Y. (2004). Functional molecular mapping of archaeal translation initiation factor 2. *J. Biol. Chem.* **279**, 15984–15993.
- Cho, S. & Hoffman, D. E. (2002). Structure of the beta subunit of translation initiation factor 2 from the archaeon *Methanococcus jannaschii*: a representative of the eIF2beta/eIF5 family of proteins. *Biochemistry*, **41**, 5730–5742.
- Nonato, M. C., Widom, J. & Clardy, J. (2002). Crystal structure of the N-terminal segment of human eukaryotic translation initiation factor 2 alpha. *J. Biol. Chem.* **277**, 17057–17061.
- Dhaliwal, S. & Hoffman, D. W. (2003). The crystal structure of the N-terminal region of the alpha subunit of translation initiation factor 2 (eIF2alpha) from *Saccharomyces cerevisiae* provides a view of the loop containing serine 51, the target of the eIF2alpha-specific kinases. *J. Mol. Biol.* **334**, 187–195.
- Gutierrez, P., Osborne, M. J., Siddiqui, N., Trempe, J. F., Arrowsmith, C. & Gehring, K. (2004). Structure of the archaeal translation initiation factor aIF2 beta from *Methanobacterium thermoautotrophicum*: implications for translation initiation. *Protein Sci.* **13**, 659–667.
- Ito, T., Marintchev, A. & Wagner, G. (2004). Solution structure of human initiation factor eIF2alpha reveals homology to the elongation factor eEF1B. *Structure*, **12**, 1693–1704.
- Roll-Mecak, A., Alone, P., Cao, C., Dever, T. E. & Burley, S. K. (2004). X-ray structure of translation initiation factor eIF2gamma: implications for tRNA and eIF2alpha binding. *J. Biol. Chem.* **279**, 10634–10642.
- Yatime, L., Schmitt, E., Blanquet, S. & Mechulam, Y. (2005). Structure–function relationships of the intact aIF2 $\alpha$  subunit from the archaeon *Pyrococcus abyssi*. *Biochemistry*, **44**, 8749–8756.
- Nikonov, O., Stolboushkina, E., Nikulin, A., Hasenöhrl, D., Bläsi, U., Manstein, D. J. *et al.* (2007). New insights into the interactions of the translation initiation factor 2 from Archaea with guanine nucleotides and initiator tRNA. *J. Mol. Biol.* **373**, 328–336.
- Yatime, L., Mechulam, Y., Blanquet, S. & Schmitt, E. (2006). Structural switch of the  $\gamma$  subunit in an archaeal aIF2 $\alpha\gamma$  heterodimer. *Structure*, **14**, 119–128.
- Sokabe, M., Yao, M., Sakai, N., Toya, S. & Tanaka, I. (2006). Structure of archaeal translational initiation factor 2  $\beta\gamma$ -GDP reveals significant conformational change of the  $\beta$  subunit and switch 1 region. *Proc. Natl Acad. Sci. USA*, **103**, 13016–13021.
- Yatime, L., Mechulam, Y., Blanquet, S. & Schmitt, E. (2007). Structure of an archaeal heterotrimeric initiation

- factor 2 reveals a nucleotide state between GTP and GDP states. *Proc. Natl Acad. Sci. USA*, **104**, 18445–18450.
18. Adams, P. D., Grosse-Kunstleve, R. W., Hung, L. W., Ioergew, T. R., McCoy, A. J., Moriarty, N. W. *et al.* (2002). PHENIX: building new software for automatic crystallographic structure determination. *Acta Crystallogr., Sect. D: Biol. Crystallogr.* **58**, 1948–1954.
  19. Stoldt, M., Wohnert, J., Gorlach, M. & Brown, L. R. (1998). The NMR structure of *Escherichia coli* ribosomal protein L25 shows homology to general stress proteins and glutaminyl-tRNA synthetases. *EMBO J.* **17**, 6377–6384.
  20. Lu, M. & Steitz, T. A. (2000). Structure of *Escherichia coli* ribosomal protein L25 complexed with a 5S rRNA fragment at 1.8 Å resolution. *Proc. Natl Acad. Sci. USA*, **97**, 2023–2028.
  21. Berchtold, H., Reshetnikova, L., Riser, C. O., Schirmer, N. K., Sprinzl, M. & Hilgenfeld, R. (1993). Crystal structure of active elongation factor Tu reveals major domain rearrangements. *Nature*, **365**, 126–132.
  22. Nissen, P., Kjeldgaard, M., Thirup, S., Polekhina, G., Reshetnikova, L., Clark, B. F. C. & Nyborg, J. (1995). Crystal structure of the ternary complex of Phe-tRNA<sup>Phe</sup>, EF-Tu, and a GTP analog. *Science*, **270**, 1464–1472.
  23. Polekhina, G., Thirup, S., Kjeldgaard, M., Nissen, P., Lippmann, C. & Nyborg, J. (1996). Helix unwinding in the effector region of elongation factor EF-Tu-GDP. *Structure*, **4**, 1141–1151.
  24. Kaufman, R. J. (2000). The double-stranded RNA-activated protein kinase PKR. In *Translational Control of Gene Expression* (Sonenberg, N., Hershey, J. W. B. & Mathews, M. B., eds), pp. 503–527, Cold Spring Harbor Laboratory, Cold Spring Harbor, NY.
  25. Chen, J. J. (2000). Heme-regulated eIF2 $\alpha$  kinase. In *Translational Control of Gene Expression* (Sonenberg, N., Hershey, J. W. B. & Mathews, M. B., eds), pp. 529–546, Cold Spring Harbor Laboratory, Cold Spring Harbor, NY.
  26. Pavitt, G. D., Ramaiah, K. V., Kimball, S. R. & Hinnebusch, A. G. (1998). eIF2 independently binds two distinct eIF2B subcomplexes that catalyze and regulate guanine-nucleotide exchange. *Genes Dev.* **12**, 514–526.
  27. Krishnamoorthy, T., Pavitt, G. D., Zhang, F., Dever, T. E. & Hinnebusch, A. G. (2001). Tight binding of the phosphorylated alpha subunit of initiation factor 2 (eIF2 $\alpha$ ) to the regulatory subunits of guanine nucleotide exchange factor eIF2B is required for inhibition of translation initiation. *Mol. Cell. Biol.* **21**, 5018–5030.
  28. Tahara, M., Ohsawa, A., Saito, S. & Kimura, M. (2004). *In vitro* phosphorylation of initiation factor 2 alpha (aIF2 alpha) from hyperthermophilic archaeon *Pyrococcus horikoshii* OT3. *J. Biochem. (Tokyo)*, **135**, 479–485.
  29. Kabsch, W. (1993). Automatic processing of rotation diffraction data from crystals of initially unknown symmetry and cell constants. *J. Appl. Crystallogr.* **26**, 795–800.
  30. Storoni, L. C., McCoy, A. J. & Read, R. J. (2004). Likelihood-enhanced fast rotation functions. *Acta Crystallogr., Sect. D: Biol. Crystallogr.* **60**, 432–438.
  31. Brunger, A. T., Adams, P. D., Clore, G. M., DeLano, W. L., Gros, P., Grosse-Kunstleve, R. W. *et al.* (1998). Crystallography & NMR System: a new software suite for macromolecular structure determination. *Acta Crystallogr., Sect. D: Biol. Crystallogr.* **54**, 905–921.
  32. Jones, T. A., Zou, J. Y., Cowtan, S. W. & Kjeldgaard, M. (1991). Improved methods for building protein models in electron density maps and the location of errors in these models. *Acta Crystallogr., Sect. A: Found. Crystallogr.* **47**, 110–119.
  33. Bailey, S. (1994). The CCP4 suite: programs for protein crystallography. *Acta Crystallogr., Sect. D: Biol. Crystallogr.* **50**, 760–763.